

In Situ Electron Microscopy of Helium Bubble Implantation in Metal Hydrides

K. Hattar, D.C. Bufford, D. Robinson, C. Snow

Sandia National Laboratories

Albuquerque, NM 87185 and Livermore, CA 94551

Abstract

Here we investigated the microstructural response of various Pd physically vapor deposited films and Er and ErD₂ samples prepared from neutron Tube targets to implanted He via *in situ* ion irradiation transmission electron microscopy and subsequent *in situ* annealing experiments. Small bubbles formed in both systems during implantation, but did not grow with increasing fluence or a short duration room temperature aging (weeks). Annealing produced large cavities with different densities in the two systems. The ErD₂ showed increased cavity nucleation compared to Er. The spherical bubbles formed from high fluence implantation and rapid annealing in both Er and ErD₂ cases differed from microstructures of naturally aged tritiated samples. Further work is still underway to determine the transition in bubble shape in the Er samples, as well as the mechanism for evolution in Pd films.

Introduction

Pd and Er metal hydrides are used for the storage of H and its isotopes. Radioactive decay of tritium produces ³He, the accumulation of which eventually forms gas bubbles, which in turn can have detrimental effects on mechanical properties [1]. The decay of tritium occurs with a half-life of 12.3 years, so experiments studying naturally aged tritiated specimens must span years in order to accumulate sufficient amounts of ³He for bubble formation [2]. Furthermore, the added difficulty of safely examining radioactive specimens increases the desirability of alternative testing methods. *Ex situ* ion implantation of He has been used to simulate the effects of ³He accumulation in Er and ErD₂ films. Prior studies noted lattice expansion from He implantation, with ErD₂ expanding more than pure Er [3]. Previous annealing studies showed sensitive temperature and dose dependence on blister formation [3-5]. While both natural aging and *ex situ* implantation have been used successfully to study cavity formation in both Pd and Er, neither approach can monitor cavity formation and evolution in real time. Here we use *in situ* ion irradiation transmission electron microscopy techniques in an effort to provide a more fundamental understanding of the cavity formation and growth mechanisms in physical vapor deposited (PVD) Pd films and Er and ErD₂ samples prepared from neutron tube targets.

Approach

Er and ErD₂ samples were prepared from neutron tube by a FIB lift out technique using an FEI DB-235 dual beam focused ion beam/scanning electron microscope (FIB/SEM). The samples were finished with a low-kV polish [6], and placed on the same carbon coated Cu TEM grid. The Pd films investigated were either PLD or sputter deposited to a thickness ranging from nominally 25 nm to 100 nm onto a NaCl substrate. The Pd films were then made free-standing by removing desolving the NaCl substrate in water and placing the film on a 3 mm Cu or Mo TEM grid. In addition, the Pd films were also directly deposited on SiN membranes associated with the window of the TEM gas heating cell. *In situ* ion implantation with 10 keV He⁺ was performed at room temperature at a rate of 2.9×10^{13} ions cm⁻²s⁻¹ using the I³TEM facility at Sandia National Laboratories [7]. For the Er and ErD₂ samples, implantation was paused at 1, 10, and 100 minutes, corresponding to fluences of 1.7×10^{15} , 10^{16} , and 10^{17} He⁺ ions cm⁻², and still images were collected. After implantation, *in situ* annealing to a nominal temperature of 790 °C was performed using a Philips CM30 TEM and a Gatan heating stage. Finally, post-annealing selected area

electron diffraction (SAD) was performed using a JEOL 2100. Similarly, the Pd films were implanted with 10 keV He until bubble structures or platelets were observed and the samples were subsequently annealed till grain growth occurred.

Results and Impacts

This result section shows TEM micrographs taken of the Er and Pd samples taken of as-prepared samples, *in situ* He implantation, and *in situ* annealing experiments. For many of the *in situ* TEM experiments, accompanying video records are also available upon request. Figure 1a shows a triple junction in the ErD₂ sample before implantation. Small bubbles were apparent at the lowest observed fluence of 1.7×10^{15} ions cm⁻². These bubbles appeared both at grain boundaries, as well as within grains and were approximately 0.4 nm in diameter. Increasing fluence to 1.7×10^{16} and 10^{17} ions cm⁻² caused a slight increase in bubble diameter to around 0.5 nm. Bubble density may have increased, although it is difficult to ascertain from the images due to the large amount of strain contrast present.

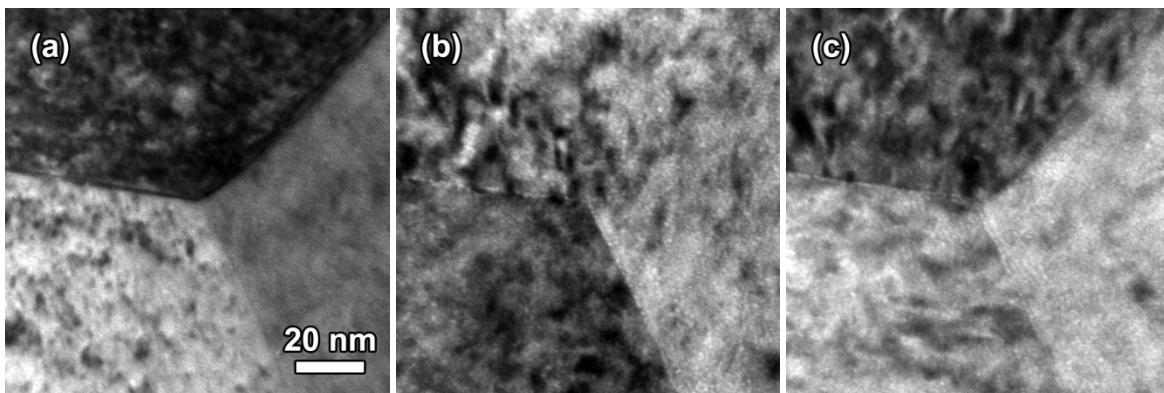


Figure 1: Triple junction in ErD₂ (a) before implantation and (b,c) after 1.7×10^{15} and 1.7×10^{17} He⁺ cm⁻² (under-focused to aid in bubble identification).

In situ heating experiments were performed with an initial heating rate of ~ 39 °C min⁻¹. Few microstructural changes were observed until a nominal temperature of 786 °C. At this point cavities appeared rather suddenly, and some cavity movement was noted. Figure 2a-d shows the formation of a larger cavity in ErD₂ during *in situ* annealing. In this image sequence, the light colored dot in the center remains essentially static as a reference point. Over a period of several seconds, a number of cavities appear in the viewing area. The cavity just above the center in 2b appears to join with another cavity in 2c, resulting in the larger cavity in 2d. After a few minutes, the microstructure stabilized and no more changes were seen. Figure 2e shows a few cavities tens of nm in diameter after annealing. However, in Figure 2f it is apparent that smaller cavities on the order of a few nm remain in the grains and along a grain boundary.

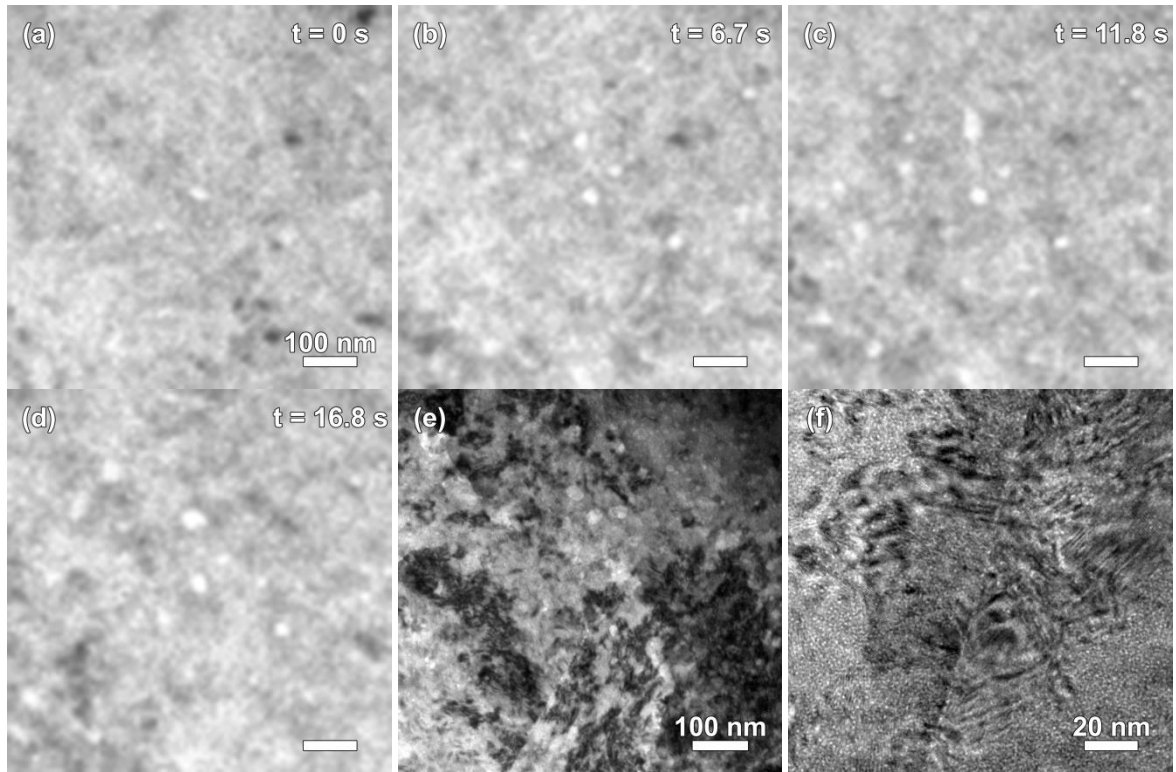


Figure 2: (a-d) Cavity formation and growth during *in situ* annealing at a nominal temperature of 786 °C. (e,f) Low and higher magnification under-focused images of cavities in ErD_2 after annealing. A grain boundary runs through the middle of (e).

It should be noted that the actual temperature of the sample during *in situ* annealing may have been lower than the temperature recorded by the instrument. The temperature is measured from a thermocouple mounted to the holder, and the samples were suspended on a carbon film, not in close thermal contact with the Cu TEM grid.

As mentioned previously, the samples were mounted on the same Cu TEM grid. While this did not allow both samples to be viewed simultaneously, it ensured that both samples experienced identical irradiation and annealing conditions. The microstructural changes resulting from implanting and annealing pure Er samples under identical conditions appear in Figure 3. Qualitatively, the Er sample behaved similarly to the ErD_2 sample, but there were a few notable differences. The small cavities present in ErD_2 after implantation were not readily visible in Er (Figure 3b). After annealing, however, cavities had formed throughout the Er sample, as shown in Figure 3c.

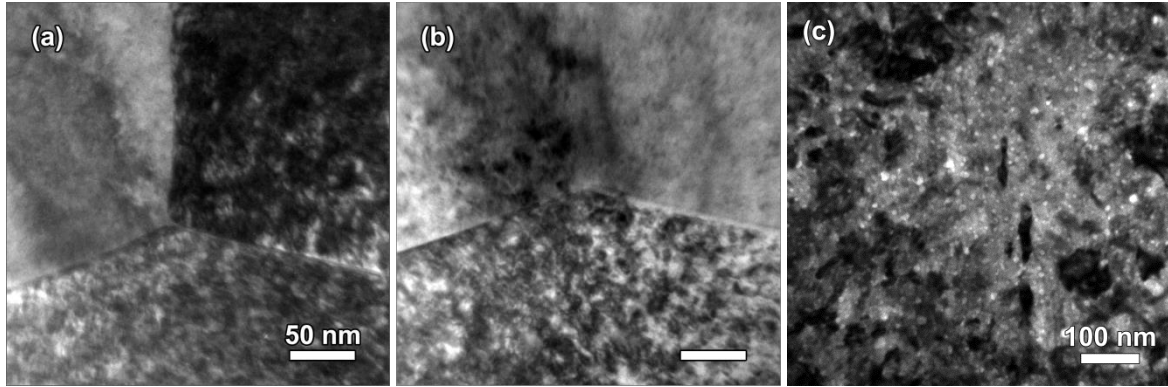


Figure 3: Triple junction in Er (a) before and (b) after $1.7 \times 10^{17} \text{ He}^+ \text{ cm}^{-2}$, and before annealing. (c) Slightly lower magnification under-focused image showing cavities in Er after *in situ* annealing. Conventional TEM imaging and over/under focusing techniques were able to identify the presence of cavities, however, strain contrast produced a significant amount of features throughout the samples, obscuring other details of the microstructure. Figure 4 shows bright- and dark-field STEM (BF- and DF-STEM) images of Er and ErD₂ after implantation and annealing. In the DF-STEM images the cavities appear particularly well defined, and can be better analyzed.

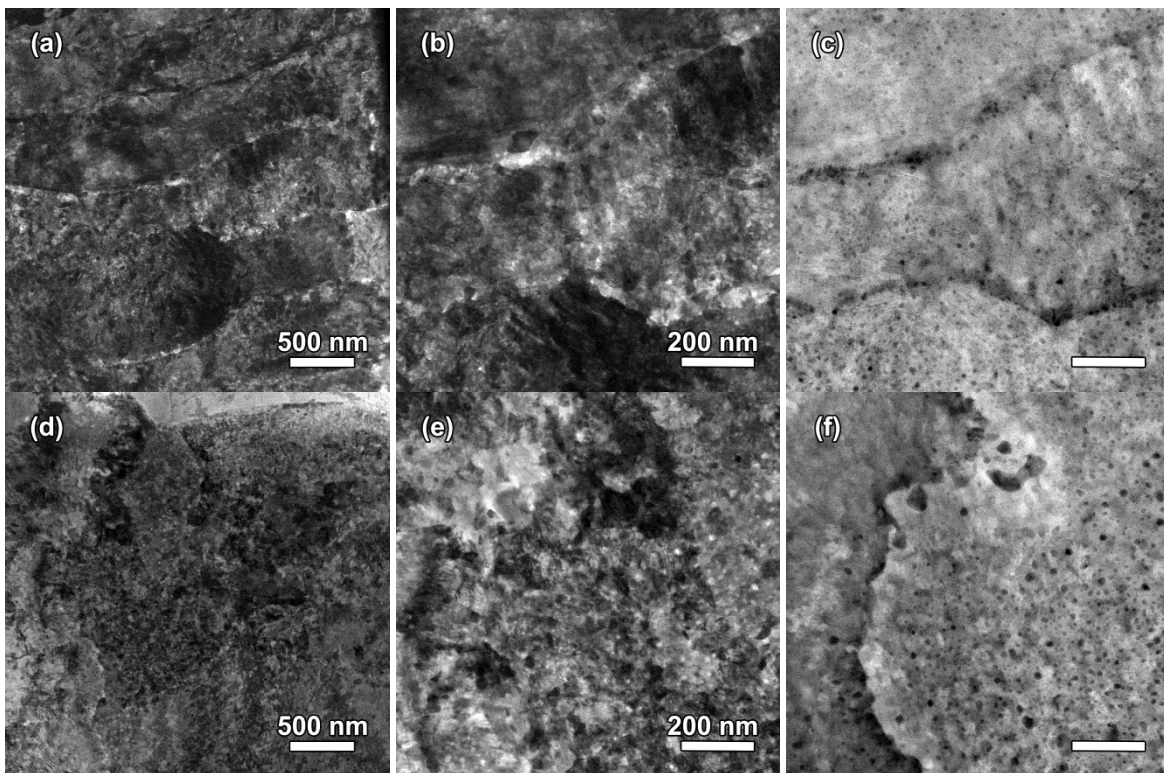


Figure 4: STEM images of Er and ErD₂ after implantation and annealing. (a) Low magnification BF-STEM image showing an overview of the Er microstructure. (b,c) Higher magnification BF- and DF-STEM images, both of the same area. (d-f) Corresponding images taken from the ErD₂ sample.

Er samples prepared by the FIB lift-out technique have previously been found to be similar to those prepared by grinding/polishing/ion mill methods [2, 6]. For the purposes of cavity formation, He and D are acceptable surrogates for ³He and T.

TRIM simulations [8] were performed to estimate the ranges and scattering of He ions during implantation into Er. Simulations of a 500 nm Er layer with 10 keV He beam at normal incidence indicated an average end of range of 70 nm. During experiments in the TEM, the beam was oriented with an angle of incidence 60° from the sample surface normal. Simulations with this geometry into a 100 nm thick Er layer predicted that 49% of ions were backscattered, 11% were transmitted, indicating that 40% were trapped within the layer, while approximately 26 vacancies ion^{-1} were produced. Thus, a considerable amount of He is expected to remain within the implanted samples. Annealing temperatures for cavity coalescence were considerably higher than those reported previously in the literature [3-5]. This is likely due to the thermal contact issue.

The structure of cavities formed by tritium aging was significantly different from that of the ion irradiated samples. Previous studies found plate-shaped bubble structures in aged films [2]. However, the samples in this work developed rounded bubbles. Tritium decay produces ^3He with an energy too low to cause lattice damage. In contrast, ion implantation of He resulted in significant vacancy production.

It would be interesting to see if the microstructural evolution differences between naturally aged tritiated specimens and ion implanted/annealed samples still appear with different experimental parameters. Particular changes of interest to the *in situ* implant procedure include lower dose rates and total doses, or elevated sample temperature to reduce accumulated lattice damage. For the *in situ* annealing experiments, desirable changes include different sample mounting for improved thermal contact, slower temperature increase rates, and longer annealing periods closer to temperatures reported for He release in previous studies (*i.e.* $\sim 400^\circ\text{C}$).

In a similar fashion to the Er systems, Pd TEM foils were produced, *in situ* He implanted, and annealed within a TEM. The as-deposited Pd films resulted in small grain size that was shown can be annealed to control the initial grain size. This was shown for both films deposited on NaCl and made free-standing, as well as for films directly deposited onto SiN window of the gas-heating TEM cell. The set of grain sizes that are possible by this technique can be seen in Figure 5.

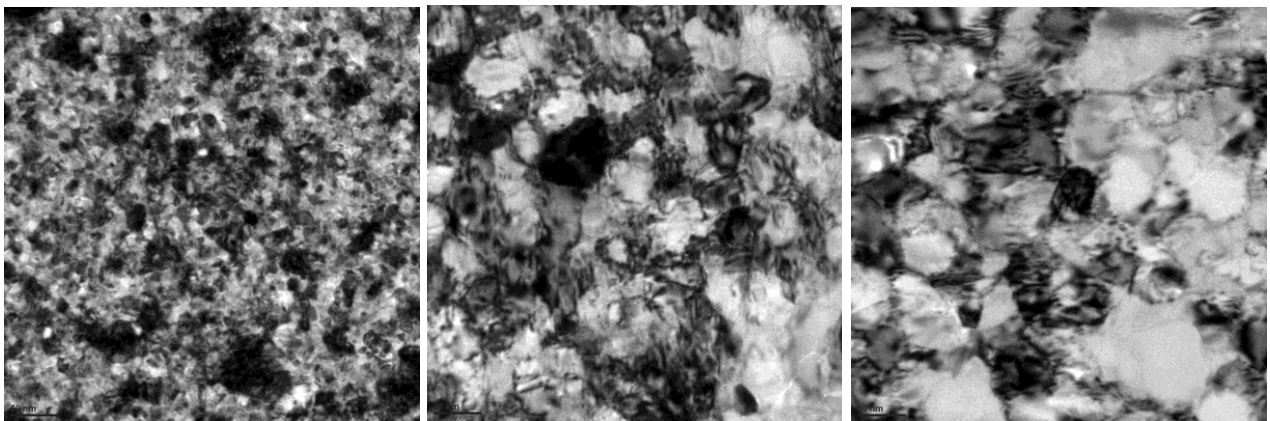


Figure 5: BF-TEM of PLD films on SiN window as a function of annealing condition.

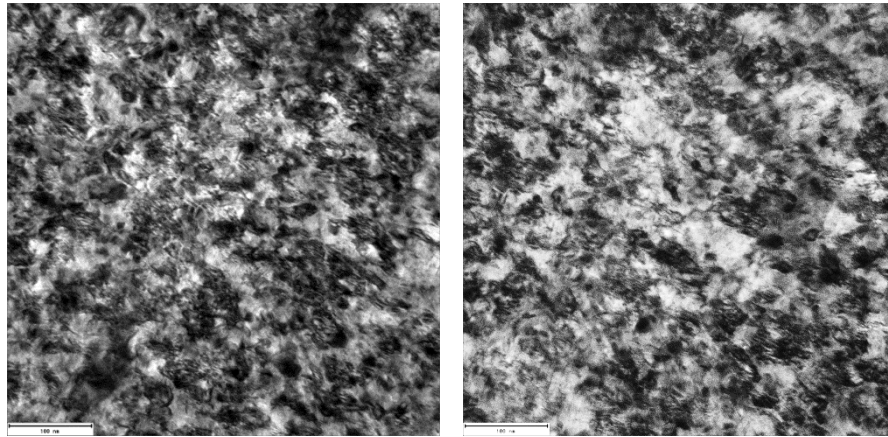


Figure 6: BF-TEM of free-standing as-deposited PLD films taken from *in situ* TEM video during 10 keV He implantation.

In a similar fashion to the Er systems, the microstructure of a single region of these films can be observed directly during *in situ* TEM 10 keV He⁺ implantation. Unfortunately, due to an error with the Faraday cup suppression at the time of the experiment, the dose could not be directly determined. Despite this limitation, structural evolution can be seen in Figure 6 and 7. In the nanostructure of the as-deposited films, little change can be seen in the microstructure. The lack of formation of He bubbles or platelets is suggestive of the idea that the nanostructure results in an increase of He transport out of the film. Further work would be needed to identify the grain size and grain boundary character of the film.

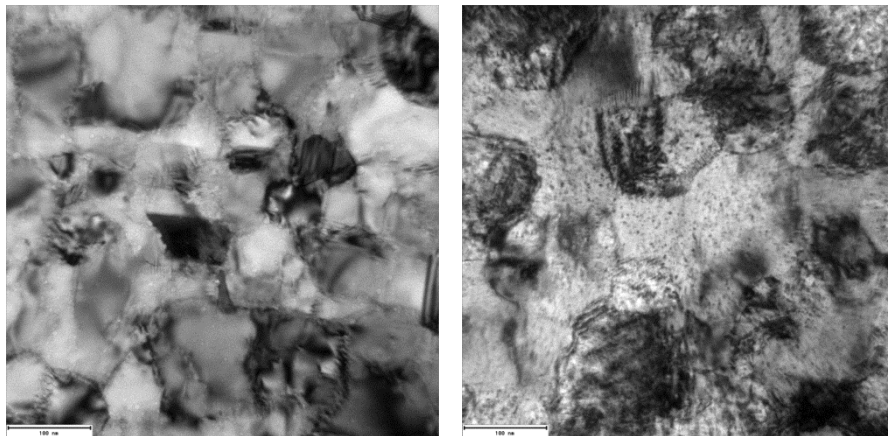


Figure 7: BF-TEM of free-standing annealed PLD films taken from *in situ* TEM video during 10 keV He implantation.

In contrast to the nanostructured Pd film, the annealed film with ultra-fine grains showed the formation of a significant density of He platelets. These are the black spots seen in Figure 7B. The density of these defects is significantly higher in Figure 7B than 6B. Although this is suggestive of the fact that He defects are less likely to form in the smaller grain structure, it is a task that is difficult to quantify due to the large amount of image contrast as a result of the high density of grain boundaries.

Conclusions and Future Work

In situ ion implantation of Er and ErD₂ samples was performed to a fluence of 1.7×10^{17} ions cm⁻². Small bubbles/cavities formed by 1.7×10^{15} ions cm⁻², growing in density but not size with increasing fluence. Post-implantation annealing to a nominal temperature of 790 °C caused the agglomeration and coarsening of these cavities. Final cavity structures differed substantially from naturally aged tritiated samples. In a similar fashion, it was shown that good quality Pd TEM samples could be prepared by PVD on NaCl substrates. It was further shown that the structure of the He bubbles could be studied through a combination of *in situ* TEM He implantation and annealing studies.

Future work is needed in the Er samples to determine the transition between spherical and planar He bubbles that occurs between the high fluence He implant and rapid annealing in comparison to natural aging of targets. For the Pd films, work is needed to determine the mechanisms active during He implantation in the films and the governing parameters. In addition, an exploratory study is needed to determine the possibility of doing *in situ* TEM He implantation in a H gas cell.

Summary of Findings and Capabilities Related to Aging

- Although previous studies showed simple rapid He implantation followed by annealing resulted in similar swelling, it was proven in this study He implantation followed by annealing did not result in the same shape bubble structures. Future work is needed to determine conditions that result in a transition in mechanisms and resulting microstructure.

References

1. Trinkaus, H. and H. Ullmaier, High-Temperature Embrittlement of Metals Due to Helium - Is the Lifetime Dominated by Cavity Growth or Crack-Growth. *Journal of Nuclear Materials*, 1994. 212: p. 303-309.
2. Snow, C.S., et al., Helium release and microstructural changes in Er(D,T)(2-x)He-3(x) films. *Journal of Nuclear Materials*, 2008. 374(1-2): p. 147-157.
3. Blewer, R.S. and J.K. Maurin, Dimensional Expansion and Surface Microstructure in Helium-Implanted Erbium and Erbium-Hydride Films. *Journal of Nuclear Materials*, 1972. 44(3): p. 260-278.
4. Blewer, R.S., Surface damage and topography of erbium metal films implanted with helium to high fluences. *Radiation Effects*, 1973. 19(4): p. 243-248.
5. Blewer, R.S. and W. Beezhold, Non linear volume expansion in helium implanted erbium metal films. *Radiation Effects*, 1973. 19(1): p. 49-52.
6. Parish, C.M., et al., Processing effects on microstructure in Er and ErD₂ thin-films. *Journal of Nuclear Materials*, 2010. 403(1-3): p. 191-197.

7. Hattar, K., D. Bufford, and D.L. Buller, Concurrent In situ Ion Irradiation Transmission Electron Microscope, in press. Nuclear Instruments & Methods in Physics Research Section B-Beam Interactions with Materials and Atoms, 2014.
8. Ziegler, J.F., M.D. Ziegler, and J.P. Biersack, SRIM - The stopping and range of ions in matter (2010). Nuclear Instruments & Methods in Physics Research Section B-Beam Interactions with Materials and Atoms, 2010. 268(11-12): p. 1818-1823.

Administrative Addendum

- **Related Publications and Presentations:**

Publication: D.C. Bufford, C.S. Snow, and K. Hattar; In situ TEM observation of He cavity evolution in Er and ErD₂; in progress

Presentation: D Bufford, C Snow, K Hattar; Bubble Formation in Er and ErD₂ During *In situ* He⁺ Ion Implantation; Microscopy & Microanalysis 2014 Hartford, CT; August 4, 2014.

- **Milestone Status:**

Quarter	Goals:	Results:
2	Identify dose and temperature conditions that result in bubble formation in Pd with minimal radiation damage in other forms	This dose and temperature conditions were determined in both PLD and sputter deposited films, as well as Er and ErD ₂ FIB prepared films.
3	Identify dose that results in bubble coalescence, and determine its dependence on temperature	This dose and temperature conditions were determined in both PLD and sputter deposited films, as well as Er and ErD ₂ FIB prepared films.
4	Extract data that can be used to validate bubble models	The evolution of implanted He evolution in this exploratory work is not the same as aged NT targets. Further work is needed to examine other implant and annealing conditions. Work is still underway to compare the He bubble evolution in implanted Pd to aged Pd samples.
4	Stretch goal: form bubbles in Pd hydride using gas cell	It was confirmed that He implantation can be geometrically achieved in the gas/heating stage. Work is still needed to perform the first experiment.